A dynamic cell recruitment process drives growth of the Drosophila wing by overscaling the Vestigial expression pattern

Luis Manuel Muñoz-Nava[1], Hugo Ariel Alvarez[2,3], Marycruz Flores-Flores[1], Osvaldo Chara[2,4] and Marcos Nahmad[1,*]

[1]Department of Physiology, Biophysics, and Neurosciences; Centre for Research and Advanced Studies of the National Polytechnical Institute (Cinvestav-IPN); Mexico City, 07360; MEXICO

[2]Systems Biology Group (SysBio), Institute of Physics of Liquids and Biological Systems (IFLYSIB); National Scientific and Technical Research Council (CONICET) and University of La Plata (UNLP); La Plata, B1900BTE; ARGENTINA

[3]Department of Biological Sciences, Faculty of Exact Sciences, University of La Plata (UNLP); La Plata, 1900, Buenos Aires, ARGENTINA

[4]Center for Information Services and High Performance Computing (ZIH); Technische Universität Dresden (TUD); Dresden, 01069; GERMANY

[*] Corresponding author's email address: mnahmad@fisio.cinvestav.mx

Running title: Cell recruitment drives growth

Key words: Organ growth; patterning; *vestigial*; cell recruitment; scaling; Drosophila wing disc.

Summary statement

Cell recruitment enhances growth of the developing Drosophila wing by expanding the expression of the wing selector gene, *vestigial*.

Abstract

Organs mainly attain their size by cell growth and proliferation, but sometimes also grow through recruitment of undifferentiated cells. Here we investigate the participation of cell recruitment in establishing the pattern of Vestigial (Vg), the product of the wing selector gene in Drosophila. We find that the Vg pattern overscales along the dorsal-ventral (DV) axis of the wing imaginal disc, *i.e.*, it expands faster than the DV length of the pouch. This overscaling cannot be explained by differential proliferation or apoptosis, nor correlates with the dynamics of the Wingless gradient, which orchestrates patterning along the DV axis. We show that Vg overscaling is recapitulated by a mathematical model that explicitly considers cell recruitment. Experimentally, when cell recruitment is genetically impaired, the Vg pattern almost perfectly scales and adult wings are 20% smaller, demonstrating that cell recruitment contributes to organ growth. Furthermore, using lineage-tracing tools, we find that cell recruitment takes place in a specific time during normal development. Altogether, our work quantitatively shows when, how, and by how much cell recruitment shapes the Vg pattern and drives growth of the Drosophila wing.

Introduction

Organ growth during development is orchestrated by morphogens, which are signaling molecules that determine gene expression in a non-cell autonomous manner and also act as mitogens (Day and Lawrence, 2000; Schwank and Basler, 2010; Dekanty and Milán, 2011; Lander, 2011; Wartlick *et al*., 2011; Bryant and Gardiner, 2016; Vollmer *et al.,* 2017). However, growth may also be driven independently of morphogen-induced cell proliferation, by a growth-by-patterning mechanism in which a differentiation pattern expands at the expense of the incorporation of undifferentiated cells. This mechanism, also known as inductive assimilation or cell recruitment, has been reported to work in both vertebrate and invertebrate development such as in the eye (Heberlein *et al.,* 1995; Strutt *et al.,* 1995) and wing discs (Baena-López and García-Bellido, 2003; Zecca and Struhl, 2007a) of the fruit fly, *Drosophila melanogaster,* as well as in the mammalian thyroid (Fagman *et al.,* 2006) and kidney (Lindström *et al.,* 2018). Little is known, however, about the dynamic properties of patterning by cell recruitment and how much organ growth can be gained through cell recruitment relative to cell growth and proliferation. These questions are generally difficult to address during normal development because the dynamics of patterning and cell proliferation occur simultaneously and it is challenging to isolate the contribution of each of these mechanisms to organ size. The Drosophila wing imaginal disc is a useful system to tackle this problem since previous studies have partly identified the molecular players of recruitment (Zecca and Struhl, 2007a; Zecca and Struhl, 2010) and genetic tools allow manipulation and quantitative assessment of patterning and growth (Hariharan and Bilder, 2006; Beira and Paro, 2016).

In Drosophila, wing fate is determined by the expression of the wing selector gene, *vestigial* (*vg*), in the pouch of the wing imaginal disc (Williams *et al.,* 1991). The absence of *vg* results in loss of wing blade identity (Williams *et al.,* 1991; Williams *et al.,* 1993), whereas ectopic expression of *vg* in other imaginal discs could induce transformation into wing-like tissue (Williams *et al.,* 1994; Kim *et al.,* 1996; Halder *et al.,* 1998; Baena-López and García-Bellido, 2003). Therefore, adult wing size depends on the size and shape of the Vg pattern established during the larval stage.

vg expression is controlled at least by two enhancers, the *vg* boundary enhancer (vg^{BE}) that responds to Notch signaling and results in high expression of Vg at the dorsal-ventral (DV) boundary (Irvine and Vogt, 1997), and the *vg* quadrant enhancer (vg^{QE}) that is partly activated by the Wingless (Wg) morphogen (Kim *et al.,* 1996; Zecca and Struhl, 2007b) resulting in a gradient of

Vg along the DV axis (Baena-López and García-Bellido, 2006). The lineage of cells abutting the DV boundary can maintain their transcriptional expression of *vg* through Polycomb/Trithorax Responsive Elements (Pérez *et al.,* 2011). The vg^{QE} is the responsive element of a cell recruitment process that depends on a feed-forward signal sent by Vg-expressing cells to non-expressing cells (Zecca and Struhl, 2007a). In 2010, Zecca and Struhl identified the following molecular details of the recruitment process (Zecca and Struhl, 2010): (1) Vg-expressing cells transcriptionally repress the protocadherin *dachsous* (*ds*), resulting in complementary patterns of Vg and Ds expression; (2) the boundary of the Vg/Ds expression domains facilitates Fat-Ds polarization, and (3) the polarization signaling induces nuclear shuttling of Yorkie (Yki), the transcriptional factor downstream of the Warts-Hippo tumor suppressor pathway, where it promotes *vg* expression transcriptionally. This process results in a new Vg-expressing cell, thus propagating the Vg pattern. As new cells are recruited into the Vg domain, the Ds pattern is pushed outwards radially by Vg-dependent transcriptional repression from the center of the wing pouch.

While previous studies have provided experimental evidence of the recruitment process by showing that Vg-expressing mosaics can induce expression of a vg^{QE} reporter non-cell-autonomously (Zecca and Struhl, 2007a; Zecca and Struhl, 2010), the contribution of cell recruitment to wild-type patterning and growth of the wing disc has not yet been investigated. Here, we precisely address this question by quantitatively examining the temporal dynamics of the Vg gradient and asking if these can be explained by a cell recruitment mechanism. We show that cell recruitment affects the shape of the Vg pattern and contributes to final size of the adult Drosophila wing.

Results

The Vg pattern overscales with respect to disc size along the DV axis

In order to investigate how the Vg pattern changes as a function of tissue size, we quantified Vg expression in wild-type wing discs during the third larval instar (85-120 h After Egg Laying (AEL) at 25˚C) as a function of DV position in a central region of the pouch delimited by the dorsal and ventral epithelial folds (Fig. 1A; Fig. S1). These folds robustly appear in the disc at about 85 h AEL at 25˚C (Sui *et al.,* 2012) and serve as references to define the length of the DV axis within the pouch area (Fig. 1A). To determine how the Vg pattern changes in discs of different sizes, we subdivided the discs into 4 groups according to their DV length, which is correlated with disc age (Fig. 1B, Fig. S2). Representative discs of each group stained for Vg and DAPI are shown in Figure

1C-F. Since fluorescence levels drop close to the folds due to tissue geometry (Fig. 1C''- F''), we used normalized DAPI levels to correct Vg expression (see Supplementary Information). After DAPI correction, Vg is expressed in a concentration gradient with maximum levels around the DV border and decreasing towards the ventral and dorsal folds in all groups (Fig. 1C'''- F'''). However, when we plotted the average of the normalized Vg patterns of each group in relative units (*i.e.*, % of DV length), we observed clear differences in Vg patterns among the groups (Fig. 1G). First, we noticed that the relative width at half maximum of the Vg gradient (width to DV length ratio) on average increases when plotted vs. DV length (Fig. 1H, Fig. S3). Note that this result is independent of how the discs were grouped and indicates that the Vg gradient overscales with respect to disc size, *i.e.*, that the Vg pattern expands further than what would be expected by uniform growth of the disc along the DV axis. Second, the Vg gradient also experiences shape changes between groups; particularly, we noticed that the slopes at the tails of the Vg gradient between groups 3 and 4 decrease, suggesting that Vg levels significantly increase in cells located at the edges of the wing pouch during the late third instar (Fig. S4). Finally, we noticed a ventral shift of the relative position of Vg maximum between groups 2 and 3 (Fig. 1I); this shift suggests that the dorsal compartment grows more than the ventral compartment during this time. In summary, we found that during normal development, the scale, shape, and symmetry of the Vg gradient changes with respect to disc size along the DV axis.

Vg overscaling cannot be accounted by the dynamics of the Wg morphogen

Since Vg expression along the DV axis depends on Wg signaling, we asked if the Vg overscaling along the DV axis is a direct consequence of a similar overexpansion of the Wg morphogen gradient. Thus, we also examined the absolute width of the Wg gradient in wing discs of different ages/sizes (Fig. 2A-D) and found that it nearly remains unchanged with respect to changes in DV length (Fig. 2E). In fact, when we plotted the relative width as a function of DV length, we found a negative correlation, *i.e.*, the Wg pattern underscales with respect to DV length (Fig. 2F, Fig. S3). Hence, we conclude that the spatial dynamics of the Wg morphogen does not explain the overscaling of the Vg pattern.

Vg overscaling cannot be explained by differential cell proliferation or apoptosis

Another plausible explanation of the overscaled Vg pattern is that there is a difference in cell proliferation or apoptosis between Vg-expressing *vs.* non-Vg expressing cells. For example, cells

near the edge of the pouch may be experiencing higher apoptosis rates or Vg-expressing cells may proliferate faster than cells outside of the Vg domain, resulting in an overscaling Vg pattern. To test these possibilities, we first examined the expression of the pro-apototic marker Caspase 3 (Cas 3) throughout development and found that apoptosis occurs at low frequency and seems to be homogeneous in the wing pouch (Fig. S5); this is consistent with a previous study (Milán *et al.*, 1997). Second, we examined cell proliferation and also confirmed the previously known result that during most of the third instar cell proliferation within the pouch is approximately uniform, except for cells at the DV boundary (Fig. S6A; Schwank *et al.,* 2011; Wartlick *et al.,* 2011; Mao *et al.*, 2013). We conclude that the overscaling of the Vg gradient cannot be accounted by differences in cell proliferation or apoptosis between cells within and outside the Vg domain.

Mathematical modeling of cell recruitment predicts the overscaling of the Vg patterns

In order to investigate if the dynamics of the Vg gradient could be accounted by a cell recruitment mechanism, we modeled the distribution of Vg in the wing pouch by means of a multi-scale model (see Supplementary Information for full description). The model combines an ordinary differential equation to account for the rate of change of Vg concentration in each cell (Vg^i) with a 2D Cellular Potts Model (CPM; Graner and Glazier, 1992; Glazier and Graner, 1993) describing the cellular dynamics (Fig. 3A and Fig. S7A, B). We assumed that cells produce Vg by two mechanisms, while there is only one sink modeled as a linear degradation. The first production term assumes that Vg expression responds to the concentration of a given non-scaling morphogen (e.g., Wg; Fig. 3A and Supplementary Information). The second cellular source of Vg is our quantitative formulation of the recruitment mechanism. In particular, we proposed that this production term depends on the difference in Vg concentration between the actual cell and the average of the concentration of its neighbors by a second order Hill function (Fig. 3A and Fig. S7C). Hence, this production term becomes relevant when the concentration of the cell is different from the one of its neighbors and negligible when they are similar. As a control, we also considered a model without the recruitment term. To account for disc growth, we explicitly included homogeneous cell proliferation in which the cell cycle parameters were fitted to the average number of cells in each of the four groups defined in Fig. 1B (Fig. S8 and Supplementary Information). Schematics of the simulated Vg expression patterns corresponding to each of the groups are shown in Fig. 3B-E (without cell recruitment) and 3B'-E' (with cell recruitment).

We examined whether the models (with and without the recruitment term) could explain the spatiotemporal expansion of Vg shown in Fig. 1 by a fitting procedure where we varied the parameter values of each of the models and minimized a target function of the residuals between experimental and simulated Vg expression data. (For simplicity, we did not take into account differences between dorsal and ventral compartments, so we only compared experimental and simulated data in the dorsal compartment; Fig. S9). The best-fit simulation of the model with recruitment reasonably recapitulates the experimental overscaling in each of the four groups (Fig. 3B''-E'', blue line *vs*. black line; Fig. S10; Video S1; Supplemental Information) and the minimum of the target function is clearly identified within the parameter space (Fig. S11A-D, blue dots, minimum marked with a green circle). In contrast, the best-fit solution of the model without the recruitment term does not reproduce the experimental data (Fig. 3B''-E'', blue line *vs*. black line; Video S1). We conclude that a model encoding a mechanism of cell recruitment can explain the overscaling dynamics of the Vg gradient.

Blocking Vg expression in ds-expressing cells disrupts the overscaling of the Vg gradient and nearly results in perfect scaling

To verify the predictions of our mathematical model, we expressed an interference RNA for *vg* (vg^{RNAi}) under *ds* control ($ds>vg^{RNAi}$) using the Drosophila Gal4-UAS system (Brand and Perrimon, 1993; Fig. S12A). Since cell recruitment works by expanding Vg expression in *ds*-expressing cells (Zecca and Struhl, 2010), we expect cell recruitment will be blocked in $ds>vg^{RNAi}$ discs. Moreover, if cell recruitment is indeed responsible for the overscaling of the Vg gradient *in vivo*, we predict that overscaling phenotype will be lost in $ds>vg^{RNAi}$ discs. We sorted the discs into four groups according to their DV length (Fig. S12B) and quantified the patterns of Vg as we did for the wild-type discs (Fig. 4A-D). As predicted, on average the overscaling property of the Vg pattern is mostly lost (Fig. 4E, compare to Fig. 1G). Although there is a small, but positive slope when we plotted the relative width of the Vg pattern *vs*. DV length in these discs (Fig. 4F), this could be attributed to the fact that vg^{RNAi} expression is not in a full knock-out of Vg-dependent recruitment. We considered if the loss of Vg overscaling in $ds>vg^{RNAi}$ discs could result from an alternative mechanism. For example, $ds>vg^{RNAi}$ discs may experience higher cell proliferation or lower apoptosis rates at the edges of the pouch due to cell competition or changes in the slope of the gradient (Baéna-Lopez and García-Bellido, 2006). However, we found that cell proliferation and apoptosis patterns are very similar in control and $ds>vg^{RNAi}$ discs (Fig. S6). We conclude that

preventing Vg expression in the *ds* expression domain blocks the recruitment-dependent overexpansion of the Vg gradient.

A time-dependent cell recruitment process contributes to the Vg pattern during normal development

In order to investigate more directly the dynamics of the cell recruitment process during normal development, we used a temperature-sensitive Gal80 (Zeidler *et al.,* 2004) to selectively mark the lineage of the cells that express *vg* through the vg^{QE} (vg^{QE} lineage) and compared it to Vg-expressing cells. We reasoned that if marking of the vg^{QE} lineage is restricted to a specific period of time during development, a cell expressing Vg and not marked by the vg^{QE} lineage will be either a cell arising from the vg^{BE} or a newly recruited cell. When we kept vg^{QE} lineage tracing constitutively active throughout development (29 ºC), as expected, nearly the whole vg^{QE} pattern is recovered (Fig. 5A-A'''). We then marked the vg^{QE} lineage from the beginning of development (29 ºC) and then switched it off (transferring the animals to 18 ºC) for 48 h (Fig. 5B-D). When we examined young third-instar discs (*i.e.* temperature switching during late second-instar / early third-instar development), no vg^{QE} lineage is marked (Fig. 5B-B'''). In contrast, when late third-instar discs were examined (*i.e.* temperature switching at mid third-instar), the vg^{QE} lineage covers the whole vg^{QE} pattern, suggesting that recruitment was already committed before this period (Fig. 5D-D'''; compare to Fig. 5A-A'''). However, when mid-to-late instar discs were examined (*i.e.* temperature switching at early-to-mid third-instar), a clear population of Vg-expressing cells at the periphery of the disc that are not within the vg^{QE} lineage can be detected (Fig. 5C-C'''). These data directly reveal that during normal wing disc development, cell recruitment takes place at a specific period of time between early and mid third-larval instar.

Impairment of cell recruitment results in smaller, but well-proportioned adult wings

We then asked whether cell recruitment could have an effect on adult wing size. Therefore, we compared $ds>vg^{RNAi}$ vs. control adult wings (Fig. 6). Most adult wings of $ds>vg^{RNAi}$ animals show the normal vein patterns (Fig. 6A-B). However, $ds>vg^{RNAi}$ wings are on average smaller than control wings (Fig. 6C). We assume that cell recruitment takes place in dorsal- and ventral-most regions of the wing pouch, which correspond to proximal regions of the adult wing. Therefore, we predicted that $ds>vg^{RNAi}$ adult wings would be smaller in proximal regions, but unaffected in distal regions. However, we found that representative areas of both proximal (Fig. 6D, inset) and distal (Fig. 6E,

inset) regions of the adult wing are similarly reduced in *ds>vg*^{RNAi} animals (17 and 21 %, respectively; Fig. 6D-E). Furthermore, we found that *ds>vg*^{RNAi} wings maintain their proximal-distal (longitudinal) to anterior-posterior (transversal) proportions, as the ratio of longitudinal to transversal dimensions is not statistically different between control and mutant adult wings (Fig. 6F). Taken together, we conclude that the impairment of cell recruitment in *ds>vg*^{RNAi} animals significantly affects adult wing size but not its proportions.

Discussion

How gene expression patterns that determine cell fate are established and contribute to organ size are important questions in developmental biology. There are two predominant models by which gene expression patterns are coordinated with organ growth. In the first model, patterns continuously depend on morphogen signaling; when the morphogen gradient changes, the patterns also change accordingly. In particular, if the morphogen scales to organ size, the patterns that depend on the morphogen would maintain their proportions relative to the final size. In the second model, a morphogen gradient establishes pre-patterns of gene expression that are then locked by positive feedback regulation. Once cells are locked in a determined fate, the final patterns are no longer dependent on the morphogen but are determined by organ growth. Particularly, when growth is uniform, this results in patterns that scale with size throughout development. In both of these models, the patterning process adjust to organ growth and the final patterns are invariant to organ size. Our data on patterning of the wing selector gene, *vg*, in the Drosophila wing disc support an additional conceptual model. After being established by Notch and Wg signaling, Vg expression is maintained through cell divisions by a mechanism involving Polycomb/Trithorax Responsive Elements. In a tissue that grows uniformly like the wing disc, this would result in a pattern that scales with tissue size. However, we find that the Vg gradient overscales relative to DV axis length (Fig. 1). This is not due to overscaling of Wg, since this morphogen actually underscales (Fig. 2), and cannot be explained by non-uniform cell proliferation or apoptosis (Figs S5, S6). Instead, our modeling results suggest that Vg overscaling could be explained by a cell recruitment mechanism (Fig. 3). In fact, when cell recruitment is genetically blocked, the overscaling phenotype is mostly lost (Fig. 4). We provide direct evidence of the cell recruitment dynamics during Vg patterning (Fig. 5). Finally, we show that cell recruitment contributes to about 20 % of adult wing size (Fig. 6).

Based on qualitative evidence on Vg expansion in genetic mosaics, Zecca and Struhl identified the molecular mechanisms of recruitment and proposed that Vg-dependent cell recruitment could contribute to growth of the Drosophila wing disc (Zecca and Struhl, 2007a; Zecca and Struhl 2010). However, it remained unclear when and to what extent cell recruitment actually contributes to normal patterning and growth of the disc. Our study directly shows that cell recruitment works by overexpanding the endogenous pattern of a selector gene, thus contributing to both patterning and organ growth. To our knowledge, this is the first study where recruited cells are directly detected during wild-type development and where its contributions to pattern formation and organ growth are quantitatively determined.

Wg signaling is absolutely required for Vg expression and propagation along the DV axis (Zecca and Struhl, 2007a). But Wg signaling is broader in early discs and then narrows (Fig. 2), which is quite opposite of the Vg overscaling dynamics here reported (Fig. 1). How can these observations be conciliated? We think that *vg* expression depends on memory of earlier, pouch-wide Wg signaling activity (Alexandre *et al.*, 2014), but Wg signaling do not play a leading role in the overscaling of Vg dynamics.

In this study, we focused on Vg patterning along the DV axis, but other signaling pathways participate in Vg expression. For example, Decapentaplegic (Dpp), a member of the BMP family, patterns the disc along the anterior-posterior (AP) axis and has been proposed an input signaling for *vg* expression (Kim *et al.*, 1996). How Dpp signaling contributes or limits cell recruitment along the AP axis and participates in the 2-dimensional Vg pattern is left to future work.

Our lineage-tracing experiments show that cells that do not come from the vg^{QE} lineage could acquire Vg expression, *i.e.* new cells get recruited, and reveal the spatiotemporal dynamics of this recruitment process (Fig. 5). We interpret these dynamics as a two-step recruitment process: The first step takes place between early and mid third-instar, and results in the overscaling of the Vg gradient width. This expansion is captured by the Vg patterns in wild-type discs (Fig. 1G,H) and is mostly lacking in $ds>vg^{RNAi}$ discs (Fig. 4E,F). The fact that this step occurs during a narrow window of time (Fig. 5), suggests that the Ft-Ds polarization signal can propagate several cells without the need of a cell-by-cell expansion of Vg expression, *i.e.* several layers of cells could begin to be recruited at once (Wortman *et al.* 2017). The second step extends from mid to late third-larval instar (about 24 hours at 25 ºC) and results in increasing levels of Vg at the tails of the gradient. This is captured by a decrease in the slopes of the Vg gradient in our timecourse examination of wild-type Vg patterns (Fig. 1G and Fig. S4). The fact that the slopes at the tails of the Vg gradient never completely flatten suggests that the rates of Vg upregulation are position-dependent, possibly

dictated by the strength of the Ft-Ds polarization which decays from its source near the DV boundary towards ventral- and dorsal-most positions. This two-step model of cell recruitment suggests that the spatial range of the process is limited by the length-scale of the Ft-Ds polarization signal.

We show that cell recruitment contributes to approximately one fifth of the total adult wing size (Fig. 6C). An interesting question that remains is to understand the purpose of cell recruitment as a growth mechanism. In other words, what is the advantage of this developmental design over simply adjusting cell sizes or cell proliferation rates to achieve a target final size? It is possible that cell recruitment plays a role in conferring some sort of robustness to developmental growth control. For example, perhaps recruitment compensates for variations in cell proliferation and could explain why final wing disc size is robust to perturbations against cell proliferation rates or cell size (Day and Lawrence, 2000).

Recent studies have showed that a cell recruitment mechanism is present in early thyroid and kidney development in mammals (Fagman et al. 2006; Lindström et al. 2018), but it is unclear how much recruitment contributes to organ growth or what are the molecular players of the recruitment signal in these contexts. Given the widespread conservation of the recruitment signal components that operate in the Drosophila wing, it would be interesting to explore whether the homologous cell recruitment signal operates as a growth-by patterning mechanism in other developing organs.

Materials and Methods

Fly stocks and genetics

The following stocks of *Drosophila melanogaster* were used: *y*, *w* provided by Fanis Missirlis (Cinvestav, Mexico); Act5C(FRT.polyA)lacZ.nls (Bloomington Drosophila Stock Center, BDSC #51308); UAS-FLP (BDSC #8209); dppGal4 (BDSC #1553); UAS-hid ((BDSC #65403); UAS-vg^{RNAi} (Vienna Drosophila Resource Center # 16896); ds-Gal4, UAS-GFP (II) provided by Gary Struhl (Columbia University, New York, USA); vgMQ-Gal4 (II) (BDSC #8229); tubP-Gal80[ts] (II) (BDSC # 7108). All flies were grown on standard fly medium at 18°C, 25 °C or 29°C, depending on the experiment. Imaginal discs were dissected from third-instar larvae of both sexes. For normal endogenous Vg and Wg patterns quantification, the *y, w* stock was used as wild-type flies (Figs 1 and 2) and kept at 25°C during egg laid and development. For recruitment impairment (Figs 4 and 6), Gal4 driver under the promoter of *dachsous* (*ds*) gene (ds-Gal4) was used and

combined with UAS-vg^{RNAi} (for recruitment inhibition) and with the *y, w* stock (control) and were kept at 25°C during egg laid and then changed to 29°C during development to increase Gal4 system efficiency. For lineage tracing of no recruited cells (Fig. 5), in vg^{QE} expressing cells a FRT STOP cassette was removed to express LacZ marker using the FLP-FRT, Gal4 and the $Gal80^{ts}$ (temperature-sensitive) systems (see Fig. 5 for genotype).

Immunostaining

After dissection in a stereoscopic microscope (Nikon SMZ800), discs were fixed in PEM-T (PEM with 0.1% of Triton X-100) with 4% paraformaldehyde, washed 3 times and blocked in PEM-T with 0.5% of BSA (Bovine Serum Albumin) for 2 hours at room temperature. Then, samples were stained with primary antibodies at 4°C overnight at the following dilutions: rabbit anti-Vg (a gift from Sean Carroll, 1:200), mouse anti-Wg (DSHB, Cat# 4D4, 1:100) and mouse anti-βGal (Promega Cat# Z378A, RRID:AB_2313752, 1:1000) and rabbit anti-Caspase 3 (Cell Signaling Technology, Cat# 9661, 1:200). DAPI (1:1000) was used to stain nuclei. 5-ethynyl-2'-deoxyuridine (EdU) labeling was performed using the Click-iT EdU Alexa Fluor 647 Imaging Kit (Invitrogen Cat#C10340) following manufacturer instructions. Primary antibodies were detected with Alexa Fluor 488 anti-mouse and 647 anti-rabbit (1:1000). Imaging was done with a confocal microscope (Leica TCS SP8 Confocal Microscope) using a 63X oil-immersion objective.

Wing mounting

Adult flies were dehydrated overnight in 70% ethanol and then separated by gender. Wings were dissected in 50% ethanol. The isolated wings were mounted and dried in a plate at 60 °C. Imaging of adult wings was done using a bright-field microscope (Nikon eclipse Ci-L/Ci-S) using a 4X objective. Wings were dissected from female and male flies and were independently analyzed.

Quantification and Statistical Analysis

The details about the quantification of Vg (Figs 1 and 4) and Wg (Fig. 2) are provided in the Supplementary Information. All the quantifications were performed using Python 3 programming language (https://www.python.org/download/releases/3.0/). The Python packages used for quantification and statistics were NumPy (http://www.numpy.org/), pandas

(https://pandas.pydata.org/), and SciPy (https://www.scipy.org/). The statistical methods used were T-test or Mann-Whitney test for comparing pairs of parametric or non-parametric datasets, respectively, and Kruskal-Wallis for more than two non-parametric datasets.

Wing disc and adult wing quantification

Vg and Wg pattern in the wing disc were quantified as explained in Fig. S1. βGal quantification were made the same way but with the initial position in the DV boundary to the ventral fold (final position). Wing representative distances and areas were quantified using the straight line and polygon selection tools respectively in ImageJ/Fiji software (https://imagej.net/).

Simulations

All simulations were performed using Morpheus 1.9.3 software (https://imc.zih.tu-dresden.de/wiki/morpheus). The time dependence of the Vg concentration was modeled by means of an ordinary differential equation for each cell (Fig. 2A), and the tissue was modeled by a Cellular Pots Model (CPM). Examples of the .xml files used to perform simulations are provided as supplementary files.

Image processing and data visualization

All the images were processed and analyzed using ImageJ/Fiji software, the matplotlib (https://matplotlib.org/), pandas (https://pandas.pydata.org/), and NumPy (http://www.numpy.org/) python packages. The data, after being analyzed, were visualized with the seaborn (https://seaborn.pydata.org/) and Matplotlib python packages.

Acknowledgments

We thank Fanis Missirlis for critical comments on the manuscript. We also thank Nahmad and Chara labs' members for interesting discussions.

Competing interests

No competing interests declared.

Funding

This work was funded by Consejo Nacional de Ciencia y Tecnología of Mexico, CB-2014-01-236685 to M. N. and by a grant from Agencia Nacional de Promoción Científica y Tecnológica, PICT-2014-3469 to O. C. L. M. M-N. and M. F-F. are supported by CONACyT (graduate scholarship program). O.C. is a career researcher from Consejo Nacional de Investigaciones Científicas y Técnicas of Argentina.

References

Alexandre, C., Baéna-López, A. and Vincent J.P. (2014). Patterning and growth control by membrane-tethered Wingless. *Nature* **505**, 180-185.

Akaike, H. (1974). A New Look at the Statistical Model Identification. *IEEE Trans. Automat. Contr.* **19**, 716–723.

Averbukh, I., Ben-Zvi, D., Mishra, S. and Barkai, N. (2014). Scaling morphogen gradients during tissue growth by a cell division rule. *Development* **141**, 2150–2156.

Baena-López, L. A. and García-Bellido, A. (2003). Genetic requirements of vestigial in the regulation of Drosophila wing development. *Development* **130**, 197–208.

Baena-Lopez, L. A. and García-Bellido, A. (2006). Control of growth and positional information by the graded vestigial expression pattern in the wing of *Drosophila melanogaster*. *Proc. Natl. Acad. Sci.* **103**, 13734–13739.

Beira, J. V. and Paro, R. (2016). The legacy of Drosophila imaginal discs. *Chromosoma* **125**, 573–592.

Brand, A. H. and Perrimon, N. (1993). Targeted gene expression as a means of altering cell fates and generating dominant phenotypes. *Development* **118**, 401–415.

Bryant, S. V. and Gardiner, D. M. (2016). The relationship between growth and pattern formation. *Regeneration* **3**, 103–122.

Day, S. J. and Lawrence, P. A. (2000). Measuring dimensions: the regulation of size and shape. *Development* **127**, 2977–2987.

Dekanty, A. and Milán, M. (2011). The interplay between morphogens and tissue growth. *EMBO Rep.* **12**, 1003–1010.

Fagman, H., Andersson, L. and Nilsson, M. (2006). The developing mouse thyroid: Embryonic vessel contacts and parenchymal growth pattern during specification, budding, migration, and lobulation. *Dev. Dyn.* **235**, 444–455.

Graner, F. and Glazier, J. A. (1992). Simulation of biological cell sorting using a two-dimensional extended Potts model. *Phys. Rev. Lett.* **69**, 2013–2016.

Glazier, J. A. and Graner, F. (1993). Simulation of the differential adhesion driven rearrangement of biological cells. *Phys. Rev. E* **47**, 2128–2154.

Hariharan, I. K. and Bilder, D. (2006). Regulation of Imaginal Disc Growth by Tumor-Suppressor Genes in Drosophila. *Annu. Rev. Genet.* **40**, 335–361.

Heberlein, U., Singh, C. M., Luk, A. Y. and Donohoe, T. J. (1995). Growth and differentiation in the Drosophila eye coordinated by hedgehog. *Nature* **373**, 709–711.

Halder, G., Polaczyk, P., Kraus, M. E., Hudson, A., Kim, J., Laughon, A. and Carroll, S. (1998). The Vestigial and Scalloped proteins act together to directly regulate wing-specific gene expression in Drosophila. *Genes Dev.* **12**, 3900–3909.

Irvine, K. D. and Vogt, T. F. (1997). Dorsal-ventral signaling in limb development. *Curr. Opin. Cell Biol.* **9**, 867–876.

Kim, J., Sebring, A., Esch, J. J., Kraus, M. E., Vorwerk, K., Magee, J. and Carroll, S. B. (1996). Integration of positional signals and regulation of wing formation and identity by Drosophila vestigial gene. *Nature* **382**, 133–138.

Lander, A. D. (2011). Pattern, growth, and control. *Cell* **144**, 955–969.

Lindström, N. O., De Sena Brandine, G., Tran, T., Ransick, A., Suh, G., Guo, J., Kim, A. D., Parvez, R. K., Ruffins, S. W., Rutledge, E. A., et al. (2018). Progressive Recruitment of Mesenchymal Progenitors Reveals a Time-Dependent Process of Cell Fate Acquisition in Mouse and Human Nephrogenesis. *Dev. Cell* **45**, 651–660.

Milán, M., Campuzano, S. García-Bellido, A. (1997). Developmental parameters of cell death in the wing disc of Drosophila. *Proc Natl Acad Sci U S A* **94**, 5691–5696.

Mao, Y., Tournier, A. L., Hoppe, A., Kerster, L., Thompson, B. J. and Tapon, N. (2013). Differential proliferation rates generate patterns of mechanical tension that orient tissue growth. *EMBO J.* **32**, 2790–2803.

Metropolis, N., Rosenbluth, A. W., Rosenbluth, M.N., Teller, A. H. and Teller, E. (1953). Equation of state calculations by fast computing machines. *J. Chem. Phys.* **21**, 1087–1092.

Pérez, L., Barrio, L., Cano, D., Fiuza, U. M., Muzzopappa, M. and Milán, M. (2011). Enhancer-PRE communication contributes to the expansion of gene expression domains in proliferating primordia. *Development* **138**, 3125–3134.

Schwank, G. and Basler, K. (2010). Regulation of Organ Growth by Morphogen Gradients. *Cold Spring Harb. Perspect. Biol.* **2**, a001669–a001669.

Schwank, G., Tauriello, G., Yagi, R., Kranz, E., Koumoutsakos, P. and Basler, K. (2011). Antagonistic growth regulation by Dpp and Fat drives uniform cell proliferation. *Dev. Cell* **20**, 123–130.

Starruß, J., de Back, W., Brusch, L. and Deutsch, A. (2014). Morpheus: a user-friendly modeling environment for multiscale and multicellular systems biology. *Bioinformatics* **30**, 1331–1332.

Strutt, D.I., Wiersdorff, V. and Mlodzik, M. (1995). Regulation of furrow progression in the Drosophila eye by cAMP-dependent protein kinase A. *Nature* **373**, 705–709.

Sui, L., Pflugfelder, G.O. and Shen, J. (2012). The Dorsocross T-box transcription factors promote tissue morphogenesis in the Drosophila wing imaginal disc. *Development* **139**, 2773–2782.

Vollmer, J., Casares, F. and Iber, D. (2017). Growth and size control during development. *Open Biol.* **7**, 170190.

Wartlick, O., Mumcu, P., Kicheva, A., Bittig, T., Seum, C., Julicher, F. and González-Gaitán, M. (2011). Dynamics of Dpp Signaling and Proliferation Control. *Science* **331**, 1154–1159.

Williams, J. A, Bell, J. B. and Carroll, S. B. (1991). Control of Drosophila wing and haltere development by the nuclear vestigial gene product. *Genes Dev.* **5**, 2481–2495.

Williams, J. A, Paddock, S. W. and Carroll, S. B. (1993). Pattern formation in a secondary field: a hierarchy of regulatory genes subdivides the developing Drosophila wing disc into discrete subregions. *Development* **117**, 571–584.

Williams, J. A., Paddock, S. W., Vorwerk, K. and Carroll, S. B. (1994). Organization of wing formation and induction of a wing-patterning gene at the dorsal/ventral compartment boundary. *Nature* **368**, 299–305.

Wortman, J. C., Nahmad, M., Zhang, P. C., Lander, A. D. and Yu, C. C. (2017). Expanding signal-molecule wavefront model of cell polarization in the Drosophila wing primordium. *PLoS Comput. Biol.* **13**, e1005610.

Wu, S., Liu, Y., Zheng, Y., Dong, J. and Pan, D. (2008). The TEAD/TEF family protein Scalloped mediates transcriptional output of the Hippo growth-regulatory pathway. *Dev. Cell* **14**, 388-398.

Yu, F. X., Zhao, B. and Guan, K. L. (2015). Hippo pathway in organ size control, tissue homeostasis and cancer. *Cell* **163**, 811-828.

Zecca, M. and Struhl, G. (2007a). Recruitment of cells into the Drosophila wing primordium by a feed-forward circuit of vestigial autoregulation. *Development* **134**, 3001–3010.

Zecca, M. and Struhl, G. (2007b). Control of Drosophila wing growth by the vestigial quadrant enhancer. *Development* **134**, 3011–3020.

Zecca, M. and Struhl, G. (2010). A feed-forward circuit linking wingless, fat-dachsous signaling, and the warts-hippo pathway to Drosophila wing growth. *PLoS Biol.* **8**, e1000386.

Zeidler, M. P., Tan, C., Bellaiche, Y., Cherry, S., Häder, S., Gayko, U. and Perrimon, N. (2004). Temperature-sensitive control of protein activity by conditionally splicing inteins. *Nat. Biotechnol.* **22**, 871–876.

1 Figures and Figure Legends

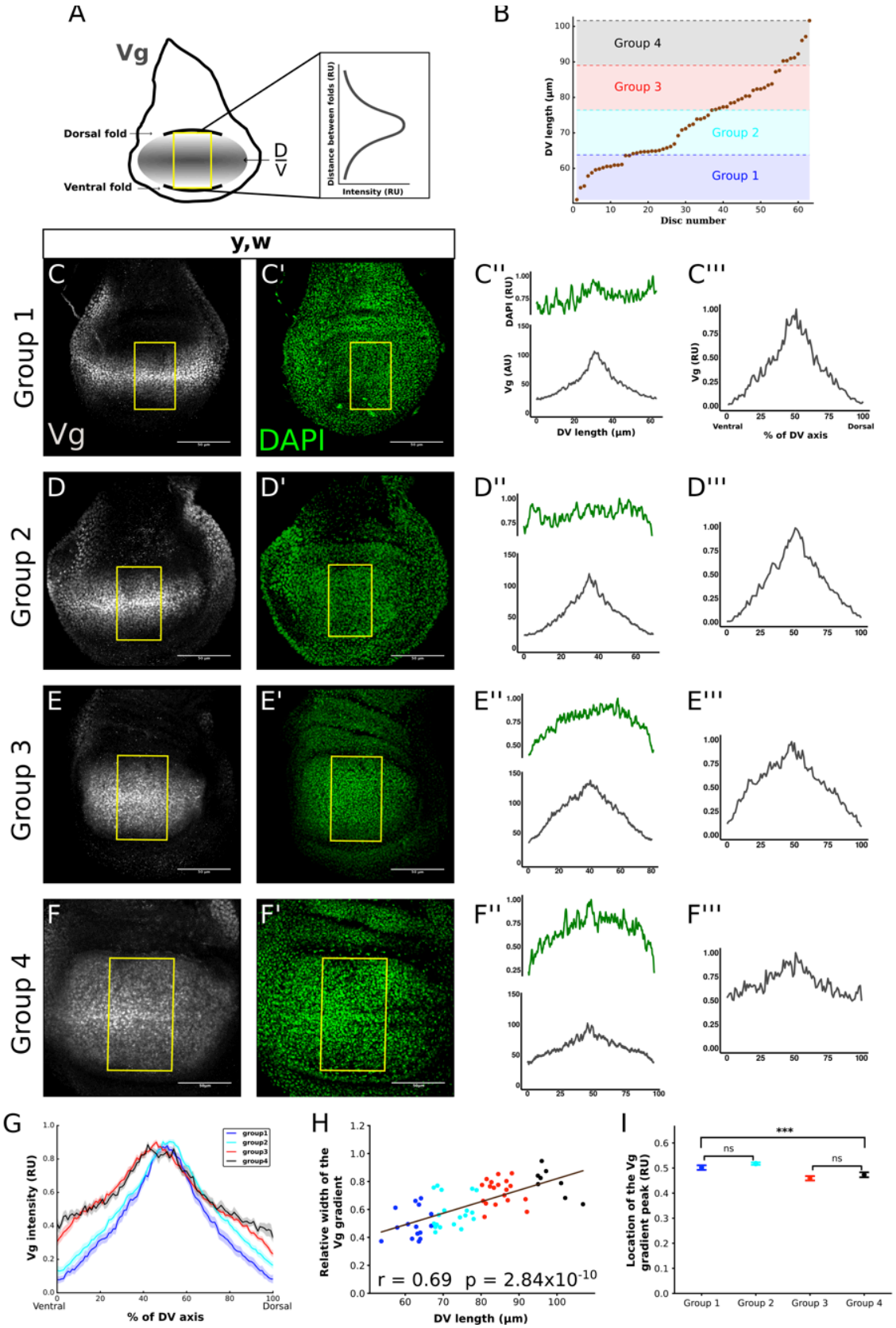

Figure 1. **Spatio-temporal quantification of Vg along the DV axis in third-instar wing discs reveals overscaling of the Vg pattern to size.** (A) Cartoon depicting the region within the wing pouch where the quantification of the Vg pattern was performed (yellow rectangle). This rectangular region is centered in the anterior posterior border of the disc and is delimited by the ventral and dorsal folds that separate the pouch from the hinge (throughout the paper, we use the distance between these folds as a measure of disc size). The intensity of Vg in each vertical line of pixels within the rectangle is averaged to obtain a spatial Vg expression along the DV axis. (B) Third-instar (ages 85-120 h After Egg Laying (AEL) at 25ºC) yellow-white (*y*, *w*) discs (throughout the study, we refer to *y*, *w* discs as wild type) are classified into four groups according to the distance between dorsal and ventral folds (DV length). The groups are defined by dividing the shortest to the longest DV length into four intervals of equal length. (C-F) Representative images of discs within each group immunostained with a Vg antibody (C-F) and DAPI (C'-F') and the quantification of the Vg patterns in the region defined in A in absolute (C''-F'') and relative (C'''-F''') units (AU and RU, respectively). (In C''-F'', the quantification of DAPI patterns (green curves in the plots on the top of each panel) in RU are shown to indicate that disc geometry could affect the intensity levels close to the folds, especially in Group 3 and Group 4 discs). The quantifications of the Vg patterns in C'''-F''' are normalized to DAPI levels (see Supplemental Information and Fig. S1). (G) Mean of the normalized Vg profiles (dark line) and Standard Error of the Mean (SEM, shaded area) from all the discs in each group (n=15, 21, 19 and 8 for Groups 1, 2, 3, and 4, respectively). (H) Relative width of the Vg gradient (defined as the width of the Vg pattern in RU at 0.5 divided by DV length) as a function of DV length; each dot in the graph corresponds to a different disc and is color-coded as in G. The solid line shows the linear regression of the data and the Pearson Correlation Coefficient, r, of the regression is displayed. The p-value corresponds to a Student-t statistical test assuming a zero-slope of the regression line as a null hypothesis. (Note that a positive slope corresponds to overscaling; a zero-slope, *i.e.*, when the null hypothesis cannot be rejected, corresponds to perfect scaling; whereas a negative slope corresponds to underscaling). (I) Comparison of the location of the Vg gradient peak in RU for the discs in each group; error bars correspond to the SEM. (Statistical significance is analyzed using a Kruskal-Wallis non-parametric test; ***, p-value$<10^{-5}$. Pairwise statistical comparisons between groups 1 and 2, and groups 3 and 4 using a Mann-Whitney non-parametric test reveal non-statistical differences between these groups; ns, p-value<0.01).

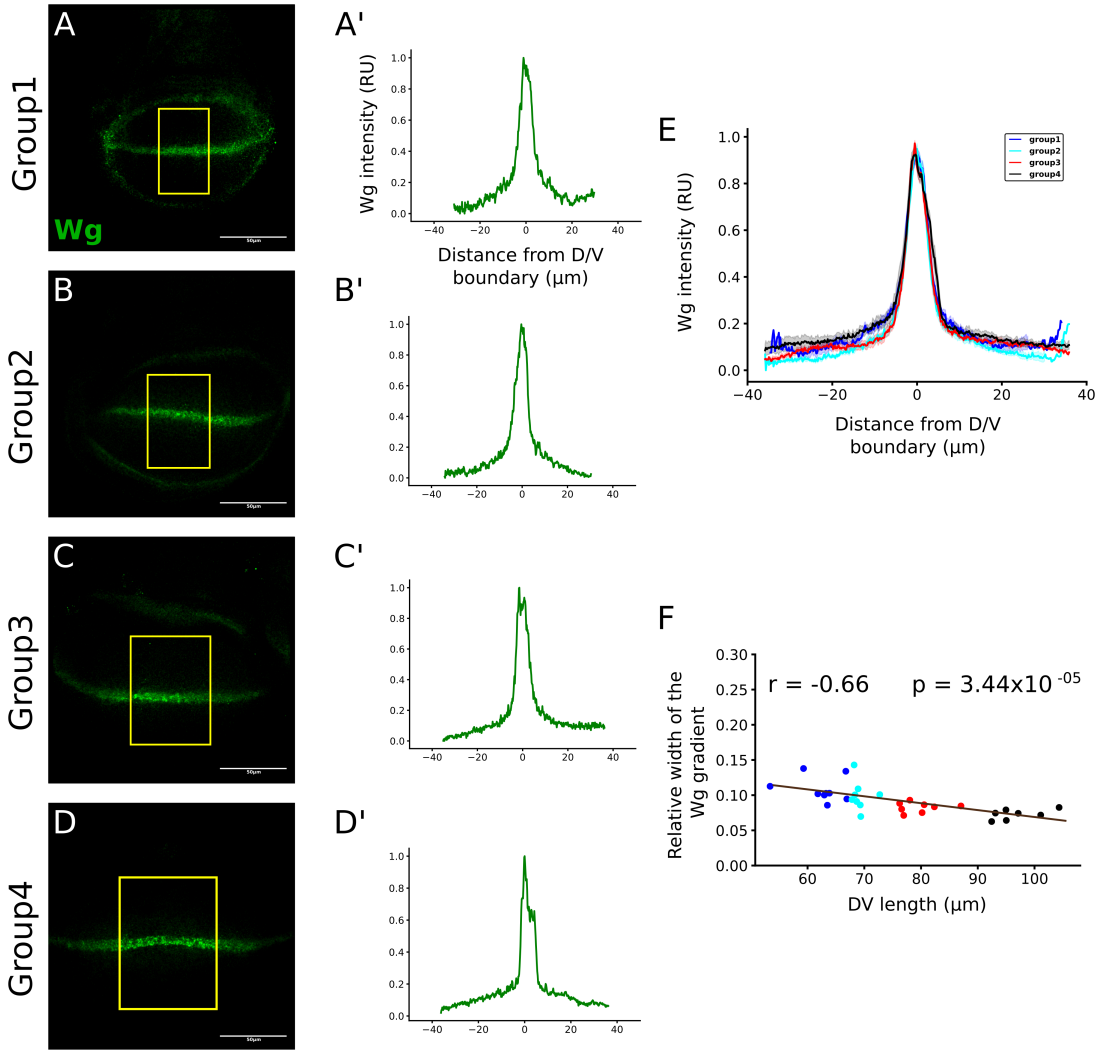

Figure 2. The pattern of the Wg morphogen underscales to disc size along the DV axis in wild-type discs. (A-D) Representative images of discs within each group immunostained with a Wg antibody (A-D) and the quantification of the gradients by horizonatlly averaging in the region defined by the yellow rectangles (A'-D'). (E) Mean of the normalized Wg profiles (dark line) and Standard Error of the Mean (SEM, shaded area) from all the discs in each group (n=9, 8, 8 and 7 for Groups 1, 2, 3, and 4, respectively). Note that unlike Fig. 1G, the units of the horizontal axis are of absolute distance to the DV boundary in order to show that the pattern does not expand significantly despite that the discs are growing, an indication of underscaling behavior. (F) Relative width of the Wg gradient (defined as the width of the Vg pattern in RU at 0.5 divided by DV length) as a function of DV length; each dot in the graph corresponds to a different disc and is color-coded as in E. The solid line shows the linear regression of the data and the Pearson Correlation Coefficient, r, of the regression is displayed. The p-value corresponds to a Student-t statistical test assuming a zero-slope of the regression line as a null hypothesis.

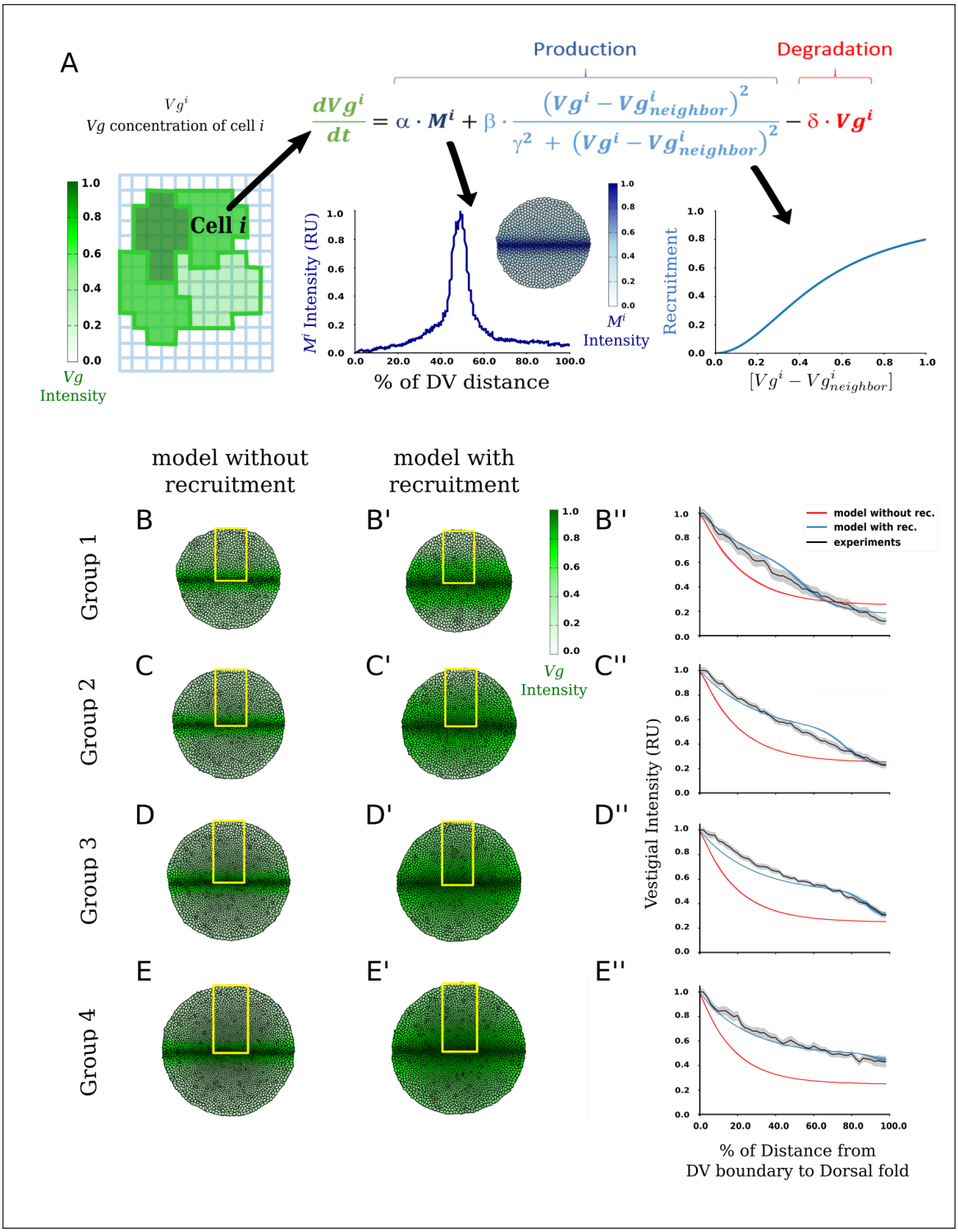

Figure 3. Multi-scale mathematical modeling with recruitment recapitulates Vg overscaling.

(A) Outline of the model (see text and Supplemental Information for further details). The dynamics

of Vg concentration in each cell is given by an ordinary differential equation including: a spatial-dependent production (first term) that models the concentration-dependent effect of a morphogen M (the representative profile shown corresponds to the experimental pattern of Wg in a representative disc), our formulation of the recruitment mechanism (second term) that depends on a Hill function of the difference in Vg concentration between the actual cell and the average of its neighbors, and linear degradation (third term). As a control, we considered a model without the recruitment term. (B-E) Simulated tissues showing Vg profiles of the model without the recruitment term (B-E), and with the recruitment term (B'-E') at four different simulated times corresponding to the average pouch areas of discs in Groups 1-4. (B''-E'') Simulated patterns of Vg in the dorsal compartment (obtained by horizontally averaging the simulated Vg patterns within the yellow rectangles in B-E and B'-E') from the model with (blue curves) or without (red curves) the recruitment term, using parameter values that best fit the average experimental Vg profiles (black curves) in Groups 1-4.

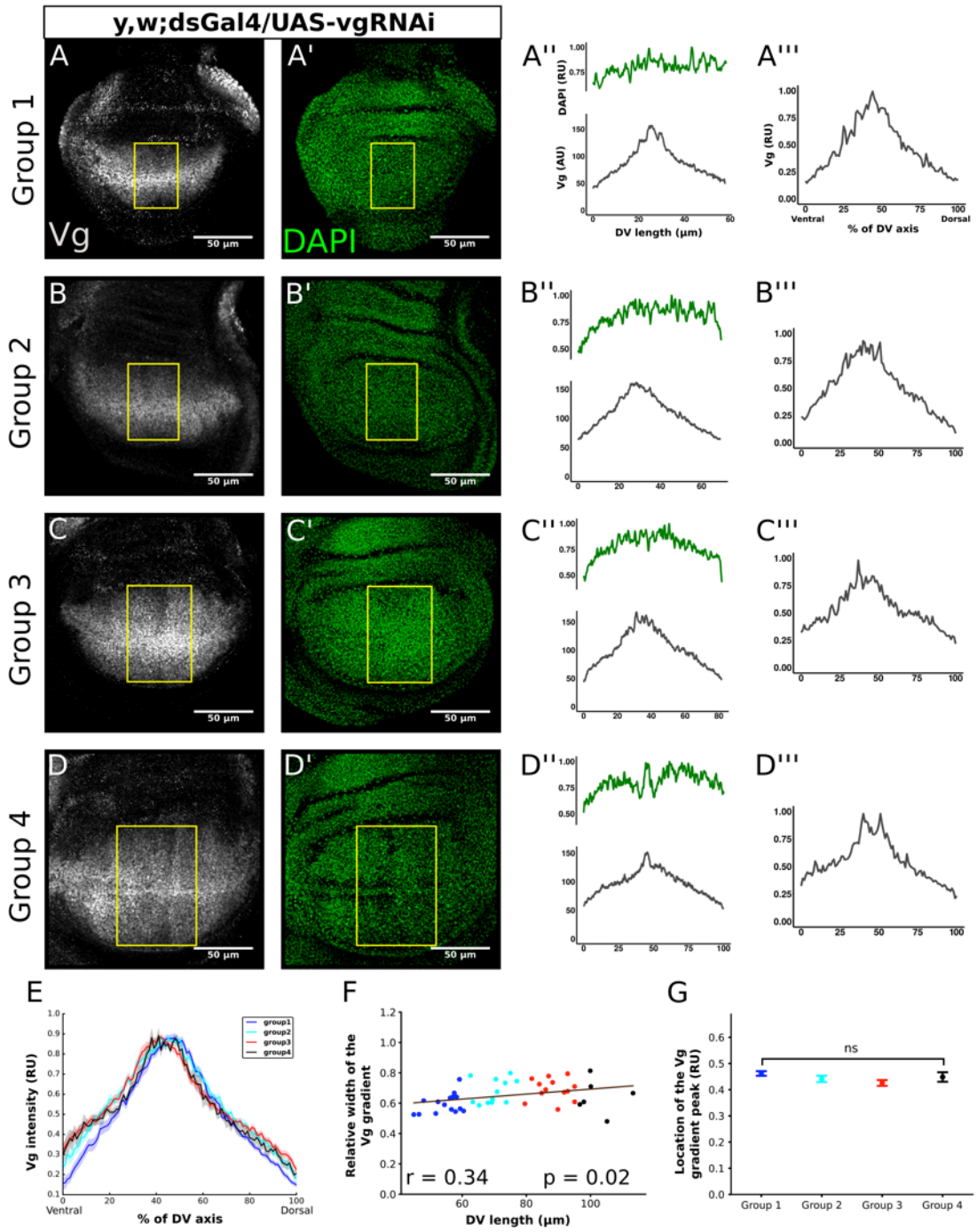

Figure 4. **Genetic impairment of cell recruitment by *ds>vg*^{RNAi} results in almost perfect scaling of the Vg pattern.** (A-D) Representative images of third-instar wing discs in which cell recruitment was blocked by expressing *vg*^{RNAi} in the domain of *ds* using the Gal4-UAS system. The discs were classified in four groups according to their DV length as defined in Fig. 1B. Discs immunostained with a Vg antibody (A-D) and DAPI (A'-D') and the quantification of the Vg patterns in a

rectangular region defined as in Fig. 1A in AU (A''-D'') and RU (A'''-D''') units as in Fig. 1. The quantifications of the Vg patterns in A'''-D''' are normalized to DAPI levels. (E) Median of the normalized Vg profiles (dark line) and SEM (shaded area) from all the discs in each group (n=15, 12, 13 and 6 for Groups 1, 2, 3, and 4, respectively). (F) Relative width of the Vg gradient (as defined in Fig. 1H) as a function of DV length; each dot in the graph corresponds to a different disc and is color-coded as in E. The solid line shows the linear regression of the data and the Pearson Correlation Coefficient, r, of the regression is displayed. The p-value corresponds to a Student-t statistical test assuming a zero-slope of the regression line as a null hypothesis. (G) Comparison of the location of the Vg gradient peak in RU for the discs in each group; error bars correspond to the SEM. (Statistical significance is analyzed using a Kruskal-Wallis non-parametric test; ns, p-value=0.075).

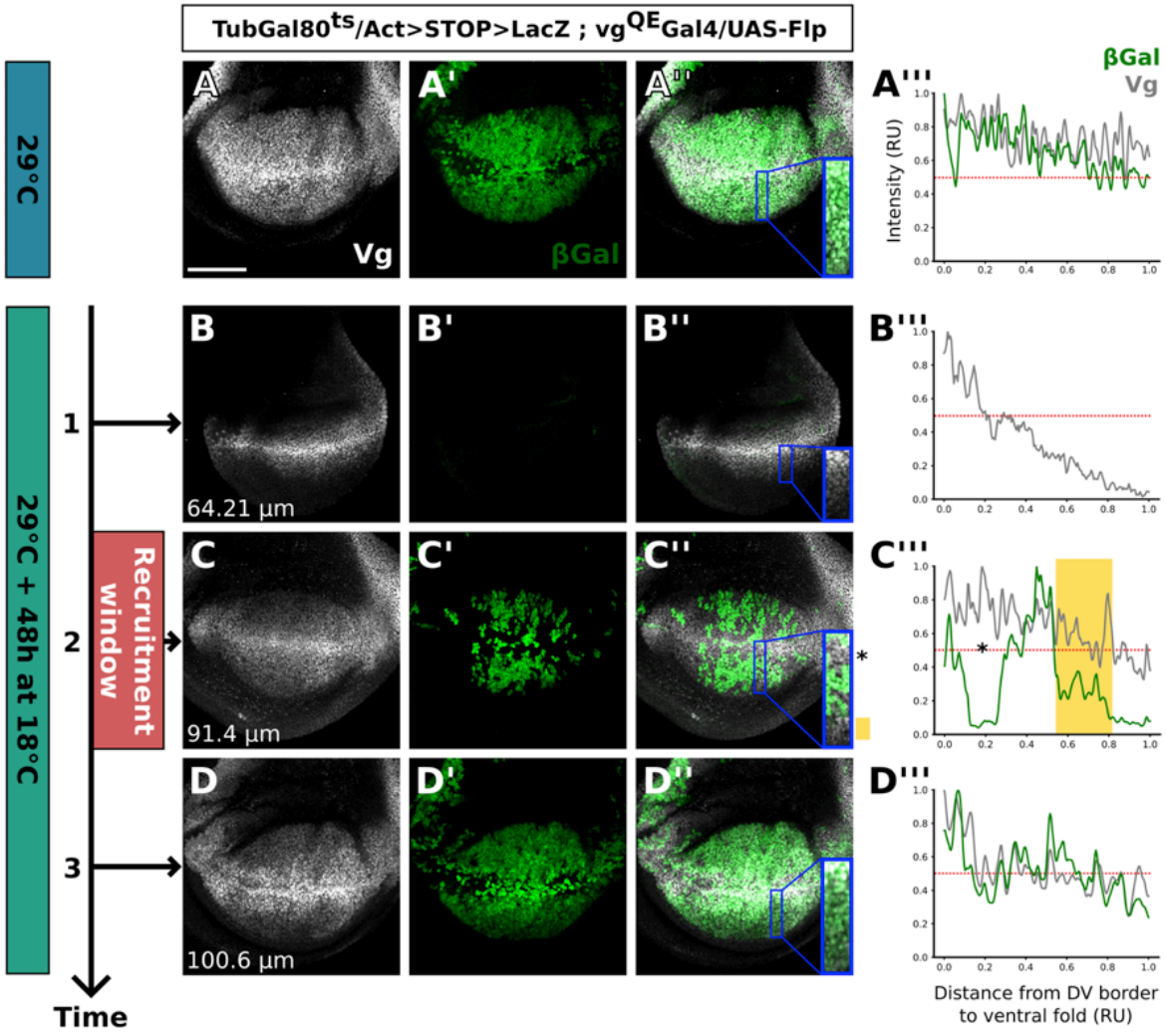

Figure 5. Lineage tracing of *vg*^{QE}-expressing cells labeled by βGalactosidase (βGal) expression and temporally modulated by Gal80^{ts}. (A-A'', B-B'', C-C'') Third instar wing discs immunostained with Vg antibody (A-D) and in which the lineage of *vg*^{QE}-expressing cells is conditionally-marked (using Gal80^{ts}) with βGal (A'-D'). At 29 ºC, Gal80^{ts} is not functional and all cells under the control of *vg*^{QE} and their progeny should express βGal, whereas at 18 ºC, Gal80^{ts} represses βGal expression. Temperature was kept at 29 ºC throughout development (A-A''; positive control), or was changed to 18 ºC for the last 48 hours before dissection of mid (B-B''), mid-late (C-C''), or late third instar larvae (D-D''). The distance between folds is depicted in the lower left corner in panels B, C, and D. (A''', B''', C''', D''') Normalized profiles of the Vg and βGal patterns in the blue rectangle area showed in A'', B'', C'', and D'', respectively. The red dotted line at 0.5 of normalized intensity serves to define which cells were recruited (yellow shaded area). Note that the region in C'' and C''' marked with an asterisk represents a region within the *vg*^{BE} and cannot considered as recruited cells. These data suggest that no recruitment is detected before the

beginning of the third instar (1) or later than mid third instar (3); we conclude that recruitment takes place in a specific window of time (red box on left), estimated between early and mid instar larval development (2).

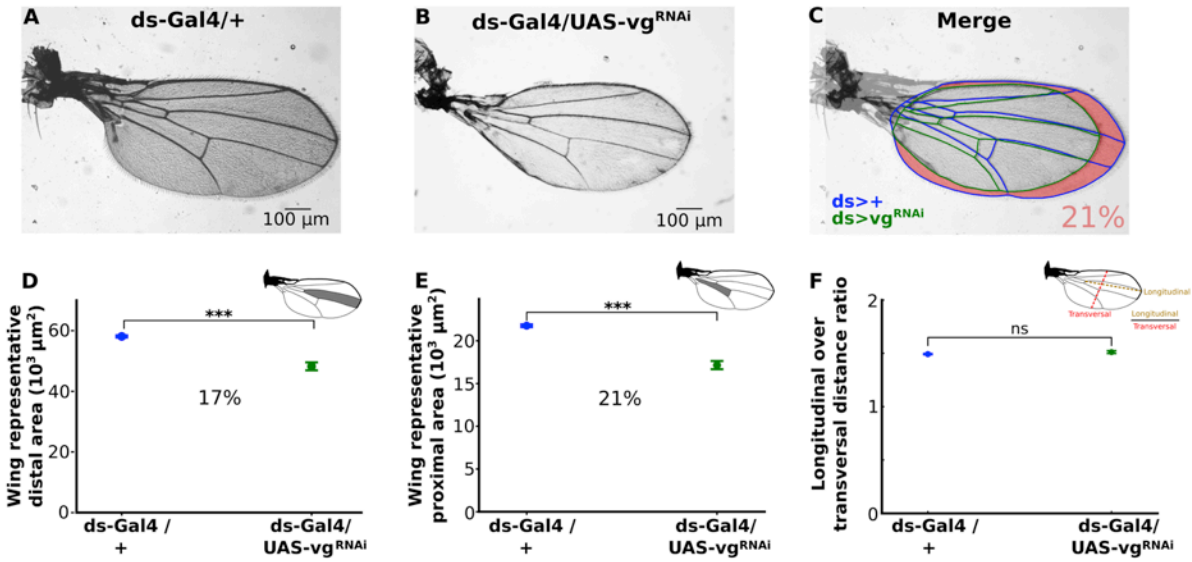

Figure 6. Genetic impairment of cell recruitment results in proportionally smaller adult wings. (A and B) Representative adult wings of *ds>vg*^{RNAi} (A) and dsGal4/+ (control, B) animals. (C) Merged wings shown in A (veins and margin colored in blue) and B (veins and margin colored in green). The area difference is shaded in pink. On average, control wings are 21% smaller than when recruitment is impaired. (D, E) Comparison of representative (see insets) distal (D) and proximal (E) areas in dsGal4/+ vs. *ds>vg*^{RNAi} wings. (Average percentage of reduction is shown, statistical significance is analyzed using a Mann-Whitney non-parametric test; ***, p-value<10^{-5}). (F) Comparison of the ratio of longitudinal to transversal distance in dsGal4/+ vs. *ds>vg*^{RNAi} wings (Statistical significance is analyzed using a Mann-Whitney non-parametric test; ns, p-value<0.01).